Title

Delineating charge and capacitance transduction in system-integrated graphene-based BioFETs used as aptasensors for malaria detection

Author names and affiliations

Gabriela Figueroa-Miranda[a,b], Yuanying Liang[a,c], Mohit Suranglikar[b], Matthias Stadler[b], Nagesh Samane[b], Marcel Tintelott[b], Young Lo[d], Julian A. Tanner[d], Xuan T. Vu[b], Joachim Knoch[e], Sven Ingebrandt[b], Andreas Offenhäusser[a], Vivek Pachauri[b*], Dirk Mayer[a*]

[a]Institute of Biological Information Processing, Bioelectronics (IBI-3), Forschungszentrum Jülich GmbH, Jülich, Germany

[b]Institute of Materials in Electrical Engineering 1, RWTH Aachen University, Aachen, Germany

[c]Institute of Polymer Optoelectronic Materials and Devices, State Key Laboratory of Luminescent Materials and Devices, South China University of Technology, Guangdong, China

[d]School of Biomedical Sciences, Li Ka Shing Faculty of Medicine, The University of Hong Kong, Pokfulam, Hong Kong Special Administrative Region

[e]Institute of Semiconductor Electronics (IHT), RWTH Aachen University, Aachen, Germany

[*]Corresponding authors: pachauri@iwe1.rwth-aachen.de; dirk.mayer@fz-juelich.de

Keywords

Malaria detection, *Plasmodium falciparum*, graphene field-effect transistor, aptasensor, aptamer-protein interaction, label-free detection.

Abstract

Despite significant eradication efforts, malaria remains a persistent infectious disease with high mortality due to the lack of efficient point-of-care (PoC) screening solutions required to manage low-density asymptomatic parasitemia. In response, we demonstrate a quantitative electrical biosensor based on system-integrated two-dimensional field-effect transistors (2DBioFETs) of reduced graphene oxide (rGO) as transducer for high sensitivity screening of the main malaria biomarker, *Plasmodium falciparum* lactate dehydrogenase (PfLDH). The 2DBioFETs were biofunctionalized with pyrene-modified 2008s aptamers as specific PfLDH receptors. While we systematically optimize biosensor interface for optimal performance, aptamer-protein transduction at 2DBioFETs is elucidated based on delineation of charge and capacitance in an updated analytical model for two-dimensional rGO/biofunctional layer/electrolyte (2DiBLE) interfaces. Our 2DBioFET-aptasensors display a limit-of-detection down to 0.78 fM (0.11 pg/mL), dynamic ranges over 9 orders of magnitude (subfemto to submicromolar), and high sensitivity and selectivity in human serum validating their diagnostic potential as rapid PoC tests for malarial management.

1. Introduction

Malaria, a vector-borne disease, continues to have a high statistical incidence with an estimated 241 million cases and up to 456000 deaths worldwide in 2020 (WHO 2021). Between protozoan vectors, *Plasmodium falciparum* and *Plasmodium vivax*, the former accounts for most deaths as a dominant malarial parasite. Malaria-attributed morbidity poses a significant public health challenge, especially in regions with underdeveloped healthcare infrastructure for prevention and care. Moreover, the emergence of new risk areas beyond the tropics makes epidemiological management of malaria a heavy burden, making eradication of malaria amongst top priority milestones by the World Health Organization (WHO 2021). Observation of parasites in blood by staining and microscopy as standard for malarial detection (Krampa et al. 2017) are unable to provide early malarial treatment. With an early treatment is estimated that almost an entirety of infections can result in positive outcomes (White et al. 2014). Rapid diagnostic test kits (RDTs) based on immunochromatographic lateral flow are used increasingly as PoC alternatives but exhibit only low to moderate sensitivity (Mouatcho and Goldring 2013). As known, most *P. falciparum* infections at the community level are associated with non-symptomatic low-density parasitemia, exposing both high and low-endemic populations to risk. Thus, it is essential to develop easily usable PoC solutions for high-sensitivity quantitative screening (Harris et al. 2010).

A promising alternative to implement quantitative screening at small footprint is to develop electrical biomolecular assays based on nanoscale ion-sensitive field-effect transistors (nanoISFETs) (Rani et al. 2016). nanoISFETs are arguably an ideal choice as transducers due to their high surface-to-volume (S/V) ratio, circumventing the need for pre-amplification steps and enabling rapid biomarker detection (Kerman et al. 2008). Graphene-based materials (GBMs) as 2D transducers facilitate distinct advantages, attributed to the highest S/V ratio, excellent electronics, and efficient bioconjugation chemistries (Jariwala et al. 2013; Mao et al. 2017; Novoselov et al. 2004; Satish Kumar et al. 2019). While ultra-low concentrations of bioanalytes including nucleic acids and proteins have been reported routinely using GBMs as transducers in complex matrices (Chen et al. 2019), detail validations of biomarker-transduction at 2D bionanointerface remained obscure mainly because of challenges related to lack of large volume 2DISFETs fabrication with high reproducibility (Andoy et al. 2018; Delle et al. 2018). In recent years, cost-effective fabrication of GBM-devices at wafer-scale offer a unique opportunity for novel 2D bionanointerfaces integration and detailed investigations of signal

transduction mechanisms (Abdolhosseinzadeh et al. 2015; Bae et al. 2010; Gao et al. 2014; Lu et al. 2018).

This work presents system-integrated reduced graphene oxide (rGO) based 2DBioFETs modified with aptamers as an optimal PoC solution for quantitative screening of malarial parasitemia while unraveling the signal transduction mechanism across rGO/electrolyte interface beyond the detection of surface charge. Carrying out elucidation of an updated analytical model for the 2D interface (2DiBLE), we show that thickness changes in the biofunctional layer (BFL) upon biomarker binding significantly influences the field-effect transport and used to determine biomarker concentration beyond surface charge. Furthermore, optimized a reliable and label-free platform for high sensitivity detection of an important malaria biomarker, *Plasmodium falciparum* lactate dehydrogenase (PfLDH), our front-end-of-line (FEoL) integrated 2DBioFETs address timely challenges in quantitative screening of infectious disease (Cheung et al. 2013). Herein, we also address practical concerns related to PoC deployment such as detection/retention time and optimal conditions for PfLDH detection, which, as shown in this work originate from fluidics design on-chip and influence the bioassay performance.

2. Materials and methods

2.1 Reagents and chemicals

PfLDH specific 2008s aptamers were modified with a pyrene functional group in order to anchor them to rGO transducer via π-π conjugation, which were synthesized by Friz Biochem GmbH (Neuried, Germany). The sequence of the aptamer is shown in Table 1. A prostate-specific antigen (PSA)-specific aptamer used as a control receptor, and human serum from male AB plasma were purchased from Sigma-Aldrich Chemie GmbH (Germany). Recombinant PfLDH and human lactate dehydrogenase B (hLDH) were obtained from bacterial expression (Cheung et al. 2013). 10 mM phosphate-buffer saline (PBS, 10 mM sodium phosphate, NaCl 0.1 M, KCl 3 mM, pH 7.5, ionic strength 115 mM) was used as buffer medium and for rinsing. 10 mM PBS with 1.0 M NaCl and 1 mM Mg^{2+}, pH 7.5, ionic strength 1022 mM) was used as medium for aptamer immobilization. All solutions were prepared using pure deionized water (18.2 MΩ cm, Milli-Q, Millipore, Merck, Darmstadt, Germany). Bovine serum albumin (BSA) was obtained from Gibco (Germany).

2.2 System-integrated 2DBioFETs

2DBioFETs were fabricated based on an earlier established process for FEoL integration of GO (Lu et al. 2018). A 2DBioFETs exhibits interdigitated design for source-drain electrodes with channel width and length of 5 and 900 µm respectively. Chips were cleaned using acetone, isopropanol (5 minutes each), rinsed with Milli-Q water, and dried in nitrogen flow. A high-temperature rapid thermal annealing (RTA) step (750 °C for 4 s) was used to achieve rGO and Ohmic contacts. The sensor chips were wire bonded onto specially designed printed circuit boards (PCBs) and a 30 µL open reservoir made of PDMS was integrated on top (Fig. S1).

2.3 2DBioFETs Biofunctionalization

PfLDH-aptamer concentration was determined by absorbance at 260 nm with the UV/Vis/NIR spectrometer Lambda 900 (Perkin Elmer, USA). The aptamer was diluted in buffer solution to a final concentration of 1 µM, which was used throughout. 30 µL solution was placed in a fluidic microwell and chips incubated at 4 °C for 16, 24, and 72 hours and afterwards rinsed thoroughly with 10 mM PBS and Milli-Q water to remove adsorbed molecules.

2.4 Electrical characterizations

Keithley semiconductor parameter analyzer model 4200 SCS and a 590 CV analyzer was used for field-effect measurements, 16 2DBioFETs on a chip were individually addressable via a common *source* and *drain* microelectrodes which were numbered virtually to establish a measurements sequence. An Ag/AgCl reference electrode (DriRef2, WPI Europe) was used as *gate*. PfLDH biomarker concentrations from 1 fM – 100 nM were prepared in 10 mM PBS (115 mM ionic strength). 30 µL sample volume was used for the biosensor measurements.

2.5 Controls and measurements in Serum

To carry out detection of PfLDH in a biological sample, measurements were performed in 10% human serum spiked with 10 fM, 10 pM, 10 nM, and 100 nM PfLDH. The added concentrations of PfLDH in serum were determined from the calibration curve and the percentage recovery of the signal was calculated.

3. Results and discussion

The concentration of PfLDH, an energy-converting enzyme in the glycolytic pathway of *Plasmodium* parasites, is known to correlate with the level of parasitemia (Moody 2002) as the malarial infection spreads in a cyclic form between humans and *Anopheles* mosquitoes (Fig. 1a). Therefore, PfLDH levels in blood serve as an ideal biomarker to manage low-level asymptomatic community-based reservoirs and symptomatic infections alike. Electrical transduction of proteins such as PfLDH which are much larger than the Debye screening limit (below 1 nm in bioelectrolyte) at a solid-liquid interface has been a topic of intrigue for ISFET based biosensors, with various interfacial modifications proposed to compensate for Debye screening and realize field-effect based detection beyond small charged molecules such as DNA strands (Tamanaha 2019). Interestingly, recent works aimed at the detection of nucleotide polymorphisms in DNA showed changes in 2DBioFETs field-effect characteristics, unexplainable with conventional surface-charge-based transduction theorem (Lanche et al. 2018). In this regard, graphene-based 2DBioFETs present a unique transducer interface, making them extremely sensitive to their environment including changes in the biomolecular conformations (Kumar et al. 2019). To elaborate further on this aspect as discussed in subsections below, we study the basic sensor characteristics of our 2DBioFETs, realize optimal rGO/BFL, systematically study the electrical transduction based on an updated 2DiBLE model considering BFL thickness changes upon PfLDH binding and simulating the field-effect transport, before deploying the platform as PoC diagnostic platform for malaria detection.

3.1 2DBioFETs characterization

Fig. 1b illustrates aptamer-modified BioFET configuration for label-free PfLDH detection. 2DBioFETs operation and bipolar transport are discussed in Fig. S2. RTA in Ar atmosphere used here to reduce GO resulted in significantly improved electrical properties in comparison to rGO devices reported by us earlier (Lu et al. 2018). Higher transconductance (g_m) ($g_{m(h)}$ = 30.0±1.6 µS and $g_{m(e)}$ = 18.4±0.8 µS) and field-effect mobility (μ_{FE}) values ($\mu_{(h)}$ = 213.4 cm^2 V^{-1} s^{-1} and $\mu_{(e)}$ = 131.0 cm^2 V^{-1} s^{-1}) were obtained with an improvement by 3 orders of magnitude. 2DBioFETs were measured in PBS of different pH and ionic strengths (Fig. S3) for determining basic sensor characteristics showing a significant shift in field-effect curves against pH at constant ionic strength. Such a shift typically is characterized by the movement of the minimum current point or Dirac point (V_{Dirac}), which was calculated from the linearly dependent pH change from 6 to 8.5 (Fig. S3c). A 23 mV/pH shift in V_{Dirac} towards positive gate voltages

(V_G) was recorded, associated with surface charge changes at rGO/electrolyte interface (Sohn et al. 2013). As reported in previous works, ion concentration change didn't influence V_{Dirac} significantly (Lanche et al. 2018; Zuccaro et al. 2015).

3.2 Aptamer immobilization and optimization

π-π conjugation of 2008s aptamers to rGO was characterized using quartz crystal microbalance with dissipation monitoring device (QCM-D) by following the process dynamically (Fig. 1c). Higher salt concentrations in PBS (1 M NaCl) favored the functionalization with significant frequency shifts and dissipation compared to low salt concentrations (100 mM NaCl) (Fig. S4a). High salt concentration can effectively reduce the repulsion among negatively charged aptamers favoring the possible exposure of the pyrene terminal group towards the rGO surface facilitating the receptor immobilization by π-π stacking interaction. A frequency shift (Δf) of 7.86 Hz and an associated dissipation shift (ΔD) of about 0.83 ppm were measured for aptamer immobilization. With aptamer functionalization, PfLDH detection was also confirmed in PBS where bovine serum albumin (BSA) was used as a blocking layer (Fig. S4b, c, and d).

The grafting density of a BFL critically influences the performance and practical operation of a biosensor (Figueroa-Miranda et al. 2020). In a stopped-flow microfluidics arrangement such as employed in this work, the aptamer's grafting density is expected to have an impact on PfLDH's mass transport and influence the sensor behavior. Fig. 1d shows sensor responses against grafting density of aptamers achieved by changing the incubation time, and characterization for successive PfLDH concentrations in 10 mM PBS. Larger signals were obtained for 2DBioFETs incubated for 16 hours, as compared to those incubated for 24 and 72 hours. For the latter, significantly smaller sensor signals are due to excessive aptamer immobilization and adsorption at the surface entailing a multilayer formation on top of the sensor, as observed by Mishyn et al. and corroborated here by AFM (Fig. S5), resulting in suboptimal analyte-receptor interaction (Mishyn et al. 2022). From here on, 2DBioFETs 16 hours of aptamers incubation were used. Atomic force microscopy (AFM) characterizations confirmed realization of BFL with significant differences in the topology with RMS surface roughness and height values of 0.19±0.03 nm / 1.02±0.05 for bare rGO, 0.48±0.03 nm / 1.05±0.06 nm for rGO+aptamer, and 0.94±0.11 nm / 4.45±0.80 nm for rGO+aptamer+PfLDH binding (Fig. 1e and Table S1).

3.3 PfLDH Signal transduction

Before discussing the influence of PfLDH interaction with BFL on field-effect transport, we ensured that there is no intrinsic drift in the field-effect characteristics by comparing it over 20 minutes in 10 mM PBS represented by black and red curves (Fig 2a). With a careful look into this graph, one can distinguish two significant trends for the subsequent field-effect measurements that represent PfLDH concentrations from 1 fM to 100 nM in 10 mM PBS. As the field-effect curves shift towards positive V_G, there is also a gradual increase in the field-effect slopes. As discussed earlier and in Fig. S3a, the shift of V_{Dirac} (Fig 3b) is representative of a net change in surface charges at the interface. Intricate effects into the restructuring of surface charges at the biointerface are revealed by the change in the field-effect slopes in addition to the shift in the Dirac point upon the biding of the successive pfLDH concentrations. Fig 2f quantifies the increment of slope as On/Off ratio, attributed to the changes associated with the restructuring of surface charges at the interface upon binding of PfLDH influencing a net increase in the electrical double layer capacitance The noticeable downshift in the field-effect curves was only observed upon PfLDH binding, which may be a cumulative effect of increased charge-carrier scattering, leakage and contact resistances. For sensor signal analysis, however, this downshift can be ignored as we compare the change in the position of the field-effect curves (i.e. Dirac point shift) and the slope of the field-effect curves.

To explain these intricate changes in the field-effect behavior, we illustrate an analytical model for the interface (2DiBLE) in Fig. 2c, which considers a negatively charged BFL on rGO attracting positively charged counter-ions on Outer Helmholtz Plane (OHP) and forming an electrical double layer (EDL) (Fig. 2c, d, and e). The BFL, composed of negatively charged aptamers (Figueroa-Miranda et al. 2021; Lenyk et al. 2020) exert a proportional change in rGO charge-carrier density upon binding of positively charged PfLDH (Figueroa-Miranda et al. 2018) following electrochemical gating (Kumar et al. 2019; Zuccaro et al. 2015). The red-colored line (Fig. 2c) shows electrostatic potential profile across 2DiBLE, for which Gouy-Chapman theory gives us the charge distribution at OHP (Lanche et al. 2018):

$$\sigma_{\mathrm{OHP}}(\psi_{\mathrm{OHP}}) = -\left(\frac{2\varepsilon_0\varepsilon_r}{l_d\beta e}\right)\sinh\left(\frac{\beta e\psi_{\mathrm{OHP}}}{2}\right) \quad (1)$$

where ψ_{OHP} is potential at OHP, $\beta = 1/k_B\mathrm{T}$, and l_d is Debye screening length, given by $l_d = \frac{2\sqrt{\varepsilon_0\varepsilon_r k_B\mathrm{T}}}{2N_A e^2 I}$. In latter the equation, I is the ionic strength of the solution; ε_0, ε_r, e are free space

permittivity, relative permittivity, and electronic charge. The electrostatic potential at 2DiBLE (ψ_0):

$$\psi_0(\psi_{\mathrm{OHP}}) = \psi_{\mathrm{OHP}} - \sigma_{\mathrm{OHP}}(\psi_{\mathrm{OHP}})/C_{Stern} \quad (2)$$

where C_{Stern} is the specific capacitance of the *Stern layer* with a thickness t_{Stern} and is given by $\varepsilon_0\varepsilon_{rStern}/t_{Stern}$. Acid-base dissociation constants (pK_a/pK_b) or isoelectric point (pI) of BFL determines the sign of charge distribution (σ_0) and potential (ψ_0) at 2DiBLE. Applying Langmuir-Freundlich theory (Heller et al. 2010) here for net charge density of BFL, charge-carrier density in rGO upon applying a particular voltage at the reference electrode can be given as

$$\sigma_{\mathrm{rGO}}(\psi_{\mathrm{OHP}}) = \psi_{\mathrm{rGO}} - \psi_0(\psi_{\mathrm{OHP}}) \times C_{BFL} \quad (3)$$

where ψ_{rGO} is the electrostatic potential of rGO. The BFL capacitance is given as $C_{BFL} = \varepsilon_0\varepsilon_{rBFL}/t_{BFL}$ with ε_{rBFL} being its relative permittivity and t_{BFL} being its thickness.

Based on 2DiBLE (Fig. 2a, b, and c), formation of the BFL at 2DBioFET would result in a V_{Dirac} shift towards negative V_{G} (Fig. S6) due to negatively charged phosphate groups of aptamers at physiological pH, while V_{Dirac} shifting positive (Fig. S6) as the PfLDH alters ψ_{rGO} at rGO/BFL interface and exerts slightly positive surface charges due to their pI of about 8.0 (Shoemark et al. 2007). Increasing PfLDH concentrations further alter ψ_{rGO} leading to the subsequent V_{Dirac} shifts (Fig. 2b).

The 2DiBLE is furthered to explain the influence of physical parameters such as permittivity ε_{rBFL} and thickness t_{BFL} on field-effect transport. To simplify, we assume a change in ε_{rBFL} as negligible whereas t_{BFL} changes after PfLDH binding (Fig. 2d, e); 2008s aptamer exhibits an average size of about 2 nm (Figueroa-Miranda et al. 2020) when folded, taken as t_{BFL} in 2DiBLE model. PfLDH estimated around 7.5 nm (Cheung et al. 2013). An increase of PfLDH concentration, therefore, may results in significant restructuring of t_{BFL} in the range of a few nanometers (Fig. 2e) which is expected to in turn alter the capacitance across 2DiBLE ($C_{BFL} = \varepsilon_0\varepsilon_{rBFL}/t_{BFL}$) associated with a gradual gain of field-effect. Further, we have validated the 2DiBLE model by simulating the field-effect response of 2DBioFET due to analyte binding and the decrease of EDLC (Fig. 2g) corroborating the experimental results.

3.4 Fluidic microwell and influence on bioassay

Fluidic microwells assembled on top of chips (Fig. S1e) facilitate bioassay measurements offering an easy and effective way for evaporation-free handling of samples. The influence of such stopped-flow fluidic on the performance of heterogeneous bioassay, however, remains underexplored. Here we evaluated the practical operation of the biosensor platform in detail and optimized it accordingly (Fig. 3). Illustration of the fluidics is shown in Fig. 3a, as top-view and side-view. For the fluidics considered here with no convection, most PfLDH molecules remain far from the capture zone i,e, aptamers at the bottom of the microwell (Fig. 3a side view). In proximity to receptors with concentration (C_{rec}), a '*boundary layer'* (BL) forms by depletion of the analytes where replenishment is reliant on a diffusion process. PfLDH concentration inside this BL (C_{bl}) is, therefore, lower than that of the present in the volume outside (C_0) the BL. The C_{bl} and C_0 relationship can be used to determine the physical regimes of mass transport. A high ratio C_{bl}/C_0 (~1.0) signifies a reaction-limited regime where receptor-analyte interaction determines the binding-constants (k_{on} and k_{off}). Conversely, a smaller value of C_{bl}/C_0 (<1.0) explains a transport-limited regime (applicable here) where parameters such as diffusion coefficient (D), sample retention time (Rt) influence the binding constants (Parsa et al. 2008).

A high C_{rec} depletes PfLDH from BL, no longer to be replenished from the bulk, lowering C_{bl}/C_0 ratio further and pushing towards a transport-controlled regime. This situation may result in a smaller signal as was seen for the highest aptamer density after 72 hours incubation time (Fig. 1d). This situation can be mitigated either by lowering C_{rec} or increasing the sample flow rate (Hartwell and Grudpan 2012) in capillary-based fluidics under a finite volume and time constraint resulting in a 'reagent-limited regime' (since $C_{bl}/C_0 \sim 1$) where binding is limited by the availability of reagents (C_s). In practical terms, at very low flow rates, a long assay time allows enough diffusion to saturate analyte binding to the receptors and enhance the biosensor signal. This also means that for high C_{rec}, minimal flow rates are favorable to achieve efficient binding resulting in larger biosensor signals. As we use a relatively high concentration (1 µM) of receptors to functionalize a capture area of ~160×10^3 µm^2 in a 3 mm diameter PDMS microwell (Fig. 3a), the stopped-flow operation is an optimal solution for PoC diagnostic, as it does not require sophisticated instrumentation. Practically, using the optimal C_{rec} and longer Rt mitigates the disadvantages of diffusion-controlled mass transport. As PfLDH diffusion in a microwell remains unchanged, we investigate the influence of Rt on bioassay as shown in Fig. 3b. The measurements start with filling microwell with 30 µL of 1 fM PfLDH in PBS and

recording the biosensor signals in a given sequence. As shown in Fig. 3a, only 9 out of 16 2DBioFETs namely S1, S4, S6, S7, S9, S10, S12, S13, and S16 were used and signals were measured at *Rt* of 6, 9, 11, 12, 14, 15, 17, 18, and 21 minutes, respectively. Similar measurements are repeated for PfLDH concentrations up to 100 nM. With an increasing *Rt*, especially beyond 12 or 13 minutes, significant signal increase represents pronounced binding. The dose-response curves for individual 2DBioFETs are plotted in the graph (Fig. 3c). Binding kinetic analysis of these curves reveals that *Rt* beyond 12 minutes for the 2DBioFETs S12, S13, S16 (purple background in Fig. 3c) also results in K_d values of around 2.4 nM, almost 10 times smaller than the values obtained for the 2008s aptamer-PfLDH interaction utilizing other transducers such as SPR (Cheung et al. 2013). From these measurement sets, it is evident that longer *Rt* with an optimal surface density of receptors may be favorable for further developments.

3.5 Bioassay in human serum

The calibration plot was obtained as a percentage of relative drain current change ($\Delta I_D/I_{D0}$) at -600 mV for PfLDH concentrations (Fig. 2a and 4a) and fit to the Langmuir-Freundlich adsorption isotherm considered an equilibrium binging model for the aptamer-protein binding complex (Ayawei et al. 2017)

$$\frac{\Delta I_D}{I_{D0}} = \frac{\left(\frac{\Delta I_D}{I_{D0}}\right)_{max} \cdot K_d \cdot c^n}{1 + K_d \cdot c^n} \tag{4}$$

where $(\Delta I_D/I_{D0})_{max}$ represents maximum signal obtained, K_d represents the equilibrium dissociation constant, c is the PfLDH concentration, and n is the index of heterogeneity. The fit to our experimental data resulted in the next parameter values $(\Delta I_D/I_{D0})_{max}$ = 13.8±1.0 % in good agreement with a measured signal value of the maximum concentration tested (100 nM), K_d = 2.4±0.36 nM, and n = 0.22±0.03, lower than one indicates a heterogeneous surface due to different affinities of the receptor on the surface of the 2DBioFET for the targets. Different affinities might originate from different DNA conformations due to intermolecular interactions among DNA molecules or receptor surface interactions. $\Delta I_D/I_{D0}$ was linearly proportional to the log concentration of PfLDH in a dynamic range of detection from 1 fM (0.14 pg/mL) to 100 nM (14 µg/mL) (Fig. 4a). The obtained sensitivity (S) was smaller (1.3 /decade) as compared with our previously reported impedimetric biosensors based on 2008s aptamer (8.3/decade, Table 1). However, the limit of detection (LOD) calculated as three standard deviations of the

control value for the 2DBioFET was 0.78 fM (0.11 pg/mL), and widen the sensor dynamic range (SDR) to nine orders of magnitude, 2 orders of magnitude extension in comparison to other electrochemical aptasensors (Table 2). The SDR reported here corresponds to a parasitemia of 0.0001% to 0.1% (<50 – 54000 parasites/µL) (Jang et al. 2013; Martin et al. 2009) giving a significant advantage for screening even low-density parasitemia in communities with endemic *P. falciparum* infections and asymptomatic cases, preventing false-negatives.

hLDH (Fig. 4c) and PSA-specific aptamers (Fig. 4d) were used as analyte and receptor controls, respectively, to evaluate and assure high selectivity and specificity of our PoC bioassay. 2DBioFET aptasensor performance was evaluated in human serum (Fig. 4b) where a blocking step with BSA was implemented to prevent any unspecific adsorption during control experiments. The PfLDH detection was determined in 10 % human serum from 10 fM to 100 nM (Fig. 4b and S7). High PfLDH recovery levels were observed in serum samples (Table S2) associated with the high specificity of the 2008s aptamer and surface blocking with BSA. It is concluded therefore that our rGO-based 2DBioFET aptasensor demonstrates superior biosensor performance down to subfemtomolar concentration of PfLDH even in a complex matrix, thereby proving their potential for real diagnostic application.

4. Conclusions

In this work, pyrene-modified 2008s aptamers, which sensitively target PfLDH, were implemented for their easier immobilization by π-π stacking on high-performance graphene-based 2DBioFETs. Several aspects for practical operation such as the influence of analyte mass-transport in passive fluidics, retention time on bioassay performance, grafting density of receptor molecules were evaluated and optimized to achieve efficient transduction and high-performance target detection in complex biological media. The intricate electrical transduction mechanism at 2D rGOBioFETs for PfLDH binding with aptamers was elucidated based on an updated 2DiBLE model including changes in the biofunctional layer thickness upon molecular binding and distinguishable influence on the field-effect transport beyond the changes in surface charge. This all optimized 2DBioFET achieved molecular detection in subfemtomolar ranges demonstrating the lowest detection limit (0.78 femtomolar) for PfLDH, outperforming other electrical 2008s aptasensors. This 2DBioFET aptasensor covers the clinically relevant range of detection for symptomatic infections and gives the possibility to manage low-level asymptomatic infections due to its superior LOD. High fidelity PfLDH detection was not only

demonstrated in buffer but also in human serum making 2DBioFET aptasensors an ideal platform for PoC deployment of malaria detection in real-world settings.

As perspectives for this 2DBioFET aptasensor, we investigate the implementation of a microfluidic cell that allows performing future continuous and dynamic response characterization.

Acknowledgments

G. F.-M. gratefully acknowledges the financial support provided by the Mexican National Council for Science and Technology and the German Academic Exchange Service (Grant number: 448904). M.S., M.T., X.T.V., S.I, and V.P. acknowledge the financial support from the DFG projects MolPro2Biosens (Grant number: 391107823), BioNanoLock (Grant number: 440055779), and from RWTH Aachen University under ERS initiative G4Neurotec (Grant number: OPSF581).

Author contributions

G. F.-M., D. M., and V. P. conceived the project. M. S. and M. T. contributed to the fabrication of the transducers. G. F.-M., Y. L., V. P., and M. S. carried out experiments and data collection under D. M., S. I., and A. O. supervision and administration. G. F.-M., D. M., N. S., X. T. V., J. K., and V. P. performed the data analysis and discussion. Y. L. and J. A. T. contributed with reagents/materials. G. F.-M., V. P., and D. M. wrote the original draft. All authors were involved in the revisions.

References

Abdolhosseinzadeh, S., Asgharzadeh, H., Seop Kim, H., 2015. Fast and fully-scalable synthesis of reduced graphene oxide. Sci Rep 5, 10160.

Andoy, N.M., Filipiak, M.S., Vetter, D., Gutiérrez-Sanz, Ó., Tarasov, A., 2018. Graphene-Based Electronic Immunosensor with Femtomolar Detection Limit in Whole Serum. Advanced Materials Technologies 3(12), 1800186.

Ayawei, N., Ebelegi, A.N., Wankasi, D., 2017. Modelling and Interpretation of Adsorption Isotherms. Journal of Chemistry 2017, 3039817.

Bae, S., Kim, H., Lee, Y., Xu, X., Park, J.S., Zheng, Y., Balakrishnan, J., Lei, T., Kim, H.R., Song, Y.I., Kim, Y.J., Kim, K.S., Ozyilmaz, B., Ahn, J.H., Hong, B.H., Iijima, S., 2010. Roll-to-roll production of 30-inch graphene films for transparent electrodes. Nature nanotechnology 5(8), 574-578.

Chen, X., Liu, Y., Fang, X., Li, Z., Pu, H., Chang, J., Chen, J., Mao, S., 2019. Ultratrace antibiotic sensing using aptamer/graphene-based field-effect transistors. Biosensors and Bioelectronics 126, 664-671.

Cheung, Y.-W., Kwok, J., Law, A.W.L., Watt, R.M., Kotaka, M., Tanner, J.A., 2013. Structural basis for discriminatory recognition of Plasmodium lactate dehydrogenase by a DNA aptamer. Proceedings of the National Academy of Sciences 110(40), 15967-15972.

Delle, L.E., Pachauri, V., Sharma, S., Shaforost, O., Ma, H., Adabi, M., Lilischkis, R., Wagner, P., Thoelen, R., Klein, N., O'Kennedy, R., Ingebrandt, S., 2018. ScFv-modified graphene-coated IDE-arrays for 'label-free' screening of cardiovascular disease biomarkers in physiological saline. Biosensors and Bioelectronics 102, 574-581.

Figueroa-Miranda, G., Chen, S., Neis, M., Zhou, L., Zhang, Y., Lo, Y., Tanner, J.A., Kreidenweiss, A., Offenhäusser, A., Mayer, D., 2021. Multi-target electrochemical malaria aptasensor on flexible multielectrode arrays for detection in malaria parasite blood samples. Sensors and Actuators B: Chemical 349, 130812.

Figueroa-Miranda, G., Feng, L., Shiu, S.C.-C., Dirkzwager, R.M., Cheung, Y.-W., Tanner, J.A., Schöning, M.J., Offenhäusser, A., Mayer, D., 2018. Aptamer-based electrochemical biosensor for highly sensitive and selective malaria detection with adjustable dynamic response range and reusability. Sensors and Actuators B: Chemical 255, 235-243.

Figueroa-Miranda, G., Wu, C., Zhang, Y., Nörbel, L., Lo, Y., Alexander Tanner, J., Elling, L., Offenhäusser, A., Mayer, D., 2020. Polyethylene glycol-mediated blocking and monolayer morphology of an electrochemical aptasensor for malaria biomarker detection in human serum. Bioelectrochemistry, 107589.

Gao, L., Ni, G.X., Liu, Y., Liu, B., Castro Neto, A.H., Loh, K.P., 2014. Face-to-face transfer of wafer-scale graphene films. Nature 505(7482), 190-194.

Harris, I., Sharrock, W.W., Bain, L.M., Gray, K.-A., Bobogare, A., Boaz, L., Lilley, K., Krause, D., Vallely, A., Johnson, M.-L., Gatton, M.L., Shanks, G.D., Cheng, Q., 2010. A large proportion of asymptomatic Plasmodium infections with low and sub-microscopic parasite densities in the low transmission setting of Temotu Province, Solomon Islands: challenges for malaria diagnostics in an elimination setting. Malaria Journal 9(1), 254.

Hartwell, S.K., Grudpan, K., 2012. Flow-Based Systems for Rapid and High-Precision Enzyme Kinetics Studies. Journal of Analytical Methods in Chemistry 2012, 450716.

Heller, I., Chatoor, S., Männik, J., Zevenbergen, M.A.G., Dekker, C., Lemay, S.G., 2010. Influence of Electrolyte Composition on Liquid-Gated Carbon Nanotube and Graphene Transistors. Journal of the American Chemical Society 132(48), 17149-17156.

Jang, J.W., Cho, C.H., Han, E.T., An, S.S.A., Lim, C.S., 2013. pLDH level of clinically isolated Plasmodium vivax and detection limit of pLDH based malaria rapid diagnostic test. Malaria Journal 12(1), 181.

Jariwala, D., Sangwan, V.K., Lauhon, L.J., Marks, T.J., Hersam, M.C., 2013. Carbon nanomaterials for electronics, optoelectronics, photovoltaics, and sensing. Chemical Society reviews 42(7), 2824-2860.
Kerman, K., Saito, M., Tamiya, E., Yamamura, S., Takamura, Y., 2008. Nanomaterial-based electrochemical biosensors for medical applications. TrAC Trends in Analytical Chemistry 27(7), 585-592.
Krampa, F.D., Aniweh, Y., Awandare, G.A., Kanyong, P., 2017. Recent Progress in the Development of Diagnostic Tests for Malaria. Diagnostics (Basel) 7(3).
Kumar, S., Kurkina, T., Ingebrandt, S., Pachauri, V., 2019. Graphene based Materials for Bioelectronics and Healthcare. Organic Bioelectronics for Life Science and Healthcare 56, 185-242.
Lanche, R., Pachauri, V., Munief, W.-M., Müller, A., Schwartz, M., Wagner, P., Thoelen, R., Ingebrandt, S., 2018. Graphite oxide electrical sensors are able to distinguish single nucleotide polymorphisms in physiological buffers. FlatChem 7, 1-9.
Lenyk, B., Figueroa-Miranda, G., Pavlushko, I., Lo, Y., Tanner, J.A., Offenhäusser, A., Mayer, D., 2020. Dual-Transducer Malaria Aptasensor Combining Electrochemical Impedance and Surface Plasmon Polariton Detection on Gold Nanohole Arrays. ChemElectroChem 7(22), 4594-4600.
Lu, X., Munief, W.-M., Heib, F., Schmitt, M., Britz, A., Grandthyl, S., Müller, F., Neurohr, J.-U., Jacobs, K., Benia, H.M., Lanche, R., Pachauri, V., Hempelmann, R., Ingebrandt, S., 2018. Front-End-of-Line Integration of Graphene Oxide for Graphene-Based Electrical Platforms. Advanced Materials Technologies 3(4), 1700318.
Mao, S., Chang, J., Pu, H., Lu, G., He, Q., Zhang, H., Chen, J., 2017. Two-dimensional nanomaterial-based field-effect transistors for chemical and biological sensing. Chemical Society reviews 46(22), 6872-6904.
Martin, S.K., Rajasekariah, G.-H., Awinda, G., Waitumbi, J., Kifude, C., 2009. Unified Parasite Lactate Dehydrogenase and Histidine-Rich Protein ELISA for Quantification of Plasmodium falciparum. The American Journal of Tropical Medicine and Hygiene 80(4), 516-522.
Mishyn, V., Hugo, A., Rodrigues, T., Aspermair, P., Happy, H., Marques, L., Hurot, C., Othmen, R., Bouchiat, V., Boukherroub, R., Knoll, W., Szunerits, S., 2022. The holy grail of pyrene-based surface ligands on the sensitivity of graphene-based field effect transistors. Sensors & Diagnostics.
Moody, A., 2002. Rapid Diagnostic Tests for Malaria Parasites. Clinical Microbiology Reviews 15(1), 66-78.
Mouatcho, J.C., Goldring, J.P.D., 2013. Malaria rapid diagnostic tests: challenges and prospects. Journal of Medical Microbiology 62(10), 1491-1505.
Novoselov, K.S., Geim, A.K., Morozov, S.V., Jiang, D., Zhang, Y., Dubonos, S.V., Grigorieva, I.V., Firsov, A.A., 2004. Electric Field Effect in Atomically Thin Carbon Films. Science 306(5696), 666-669.
Parsa, H., Chin, C.D., Mongkolwisetwara, P., Lee, B.W., Wang, J.J., Sia, S.K., 2008. Effect of volume- and time-based constraints on capture of analytes in microfluidic heterogeneous immunoassays. Lab on a Chip 8(12), 2062-2070.
Rani, D., Pachauri, V., Mueller, A., Vu, X.T., Nguyen, T.C., Ingebrandt, S., 2016. On the Use of Scalable NanoISFET Arrays of Silicon with Highly Reproducible Sensor Performance for Biosensor Applications. ACS Omega 1(1), 84-92.
Satish Kumar, Tetiana Kurkina, Sven Ingebrandt, Pachauri, V., 2019. Graphene based Materials for Bioelectronics and Healthcare. Organic Bioelectronics for Life Science and Healthcare, pp. 185-242. Materials Research Foundations.

Shoemark, D.K., Cliff, M.J., Sessions, R.B., Clarke, A.R., 2007. Enzymatic properties of the lactate dehydrogenase enzyme from Plasmodium falciparum. The FEBS Journal 274(11), 2738-2748.
Sohn, I.-Y., Kim, D.-J., Jung, J.-H., Yoon, O.J., Nguyen Thanh, T., Tran Quang, T., Lee, N.-E., 2013. pH sensing characteristics and biosensing application of solution-gated reduced graphene oxide field-effect transistors. Biosensors and Bioelectronics 45, 70-76.
Tamanaha, C.R., 2019. A Survey of Graphene-Based Field Effect Transistors for Bio-sensing. In: Kranz, C. (Ed.), Carbon-Based Nanosensor Technology, pp. 165-200. Springer International Publishing, Cham.
White, N.J., Pukrittayakamee, S., Hien, T.T., Faiz, M.A., Mokuolu, O.A., Dondorp, A.M., 2014. Malaria. The Lancet 383(9918), 723-735.
WHO, 2021. World malaria report 2021. World Health Organization: Geneva, Switzerland.
Zuccaro, L., Krieg, J., Desideri, A., Kern, K., Balasubramanian, K., 2015. Tuning the isoelectric point of graphene by electrochemical functionalization. Scientific Reports 5(1), 11794.

Figures

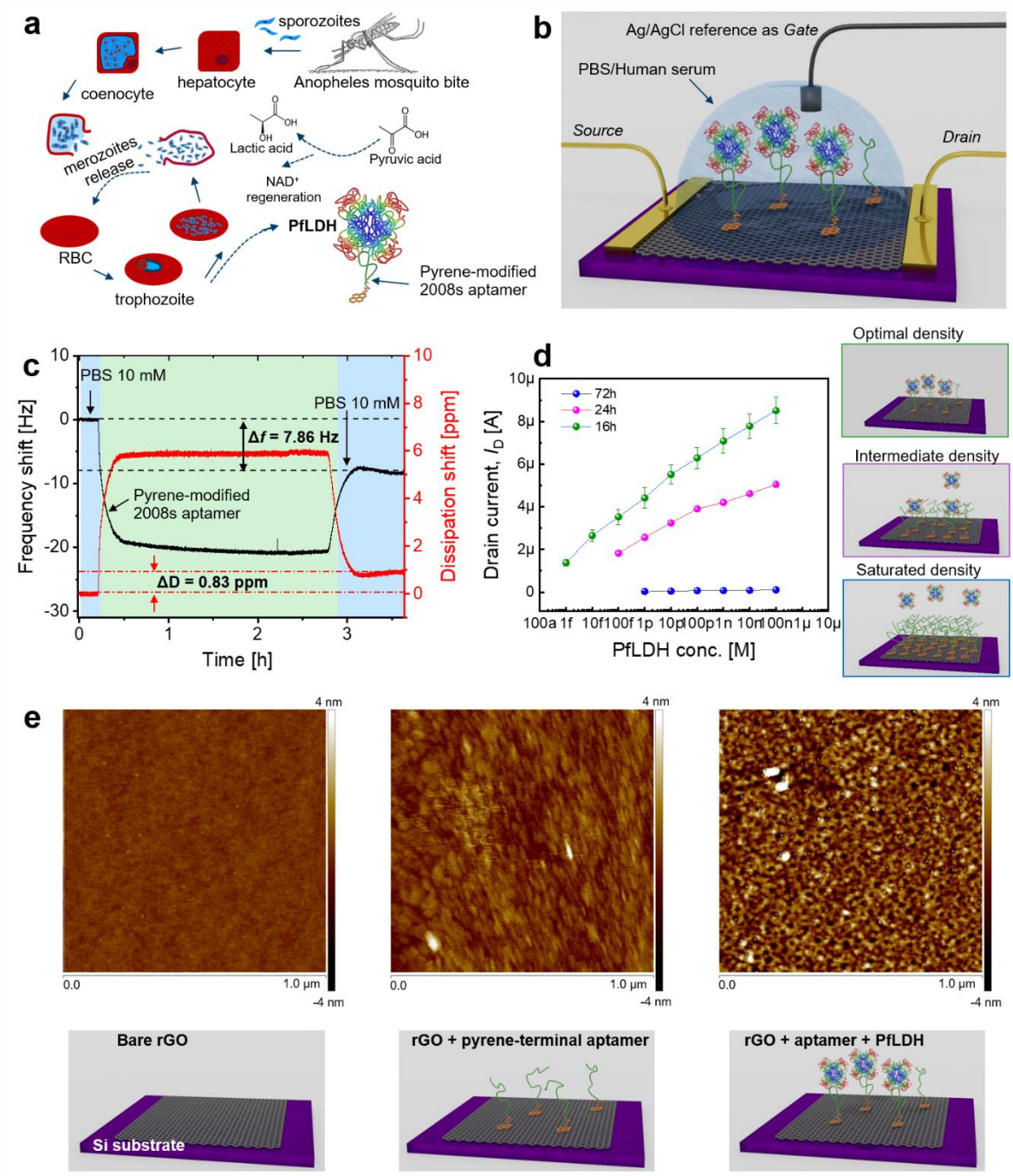

Fig. 1 Aptamer functionalization of 2DBioFETs, characterization and optimizations. **a** Schematic illustration of different stages of *P. falciparum* parasitemia in humans and the production of *Plasmodium falciparum* lactate dehydrogenase (PfLDH), the main biomarker for malaria detection. **b** Illustration of the 2DBioFET with pyrene-functionalized PfLDH specific 2008s aptamers. **c** Pyrene-modified 2008s aptamers binding to rGO substrate are characterized

using QCM-D measurements. The color background indicates the different added solutions used for rinsing or for aptamer immobilization. The dash lines represent the limits from which Δf or ΔD were calculated. **d** Graph showing the influence of aptamer's surface density on the electrical signal and dynamic range of the biosensor platform. A relative change in the drain current output (ΔI_D) at -600 mV (drain voltage, V_D = 100 mV) against the different concentrations of PfLDH was taken as the biosensor signal. Here, green, pink, and blue curves represent *in situ* recordings of the dose-response from 2DBioFETs with biofunctional layers realized after incubation of 1 µM 2008s aptamers for 16, 24, and 72 h, respectively. The PfLDH concentration tested in the dose-response analysis range from femtomolar to nanomolar concentrations in 10 mM PBS buffer. **e** Surface characterization of aptamer modified 2DBioFETs using atomic force microscopy (AFM) showing the scanned image of a bare rGO surface (left), rGO-aptamer (middle), and rGO-aptamer-PfLDH (right). (For interpretation of the references to color in this figure legend, the reader is referred to the Web version of this article.)

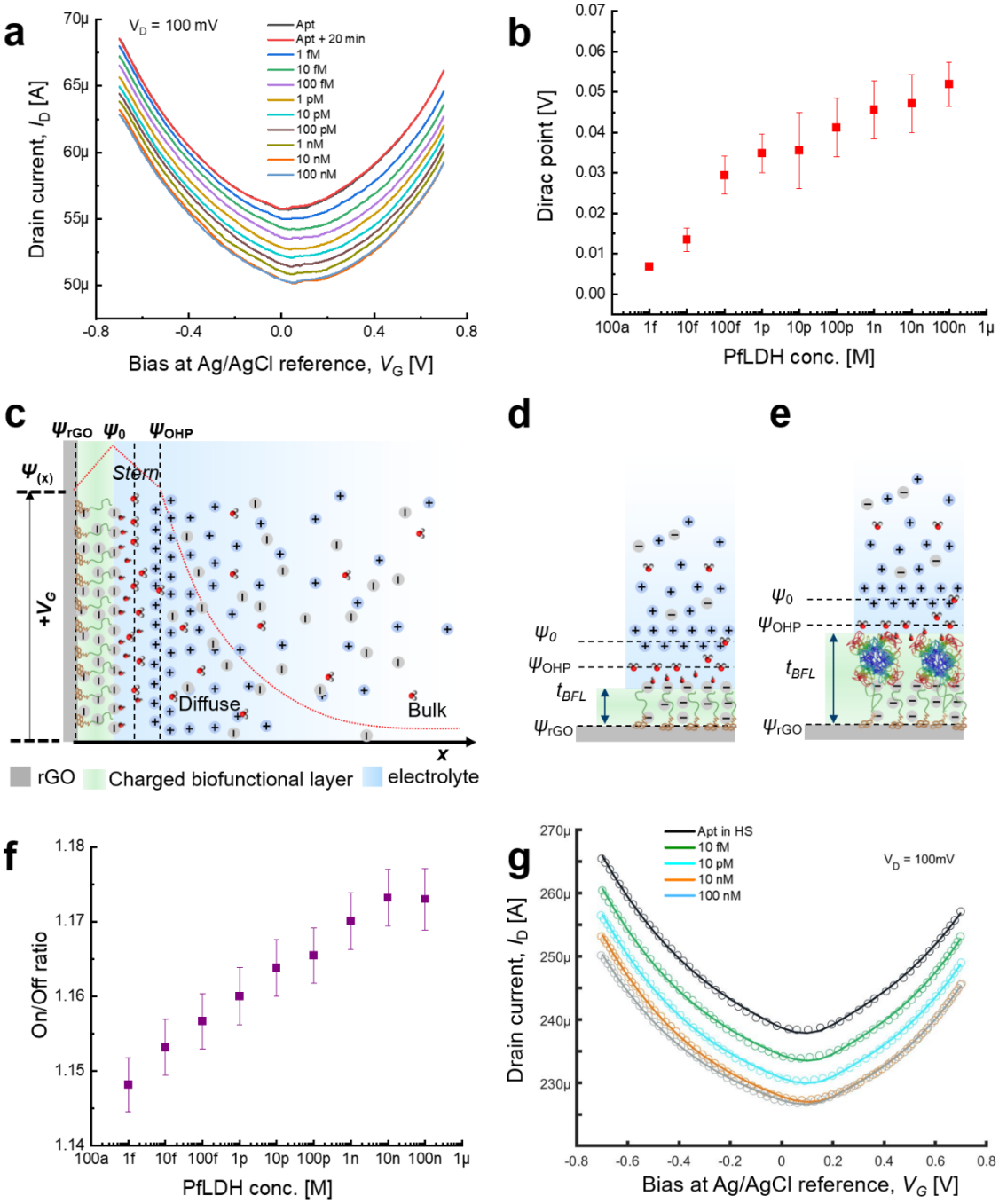

Fig. 2 Two-dimensional interface of graphene/biofunctional layer/electrolyte (2DiBLE) model and operation of biosensor platform. **a** The graph shows the field-effect-based biosensor measurements after aptamer immobilization (Apt), after passing 20 min (apt + 20 min), and after detection of several concentrations of the target PfLDH ranging from 1 fM (0.14 pg/mL) to 100 nM (14 µg/mL) in 10 mM PBS solution. The biosensor was operated at V_D = 100 mV while the bias at the Ag/AgCl reference V_G was swept at ±700 mV. **b** The graph shows

a shift in the Dirac point towards positive gate voltages while PfLDH concentrations increase signifying the change in the net surface charge density at the Graphene/Biolayer/Electrode interface. **c** Descriptive model of 2DiBLE where we include a negatively charged layer of 2008s aptamers that were immobilized onto rGO followed with the formation of inner (IHP) and outer (OHP) Helmholtz layers as well as the diffused layer. **d** Closer look into the formation of 2DiBLE when immobilized with the aptamers forming a thin immobile negatively charged layer. **e** PfLDH binding to the aptamers results in the change of surface charge density and distribution at the solid-liquid interface resulting in an altered 2DiBLE. **f** The graph plots the ratio of output current at -600 mV to the values obtained at Dirac point as On/Off ratio, while the concentration of PfLDH is increased in the buffer. The increased binding of the PfLDH as shown in **e** influences the total double layer capacitance (EDLC) across 2DiBLE, and translates into a unique trend where the slope of the field-effect curves increases with the increasing PfLDH concentrations, resulting in higher On/Off current ratio. All experiments were repeated with three different chips and nine different 2DBioFETs from each chip (n = 27). **g** The graph represents the actual experimental data (continuous line) and the simulation (circles) based on the updated model for 2DiBLE for the field-effect behavior of aptamer modified BioFETs and sensor response for relevant PfLDH concentrations. ψ_{rGO}: electrostatic potential of reduced graphene oxide (rGO); ψ_{OHP}: potential at OHP; ψ_0: potential at the rGO/BFL-Stern interface; t_{BFL}: thickness of the biofunctional layer.

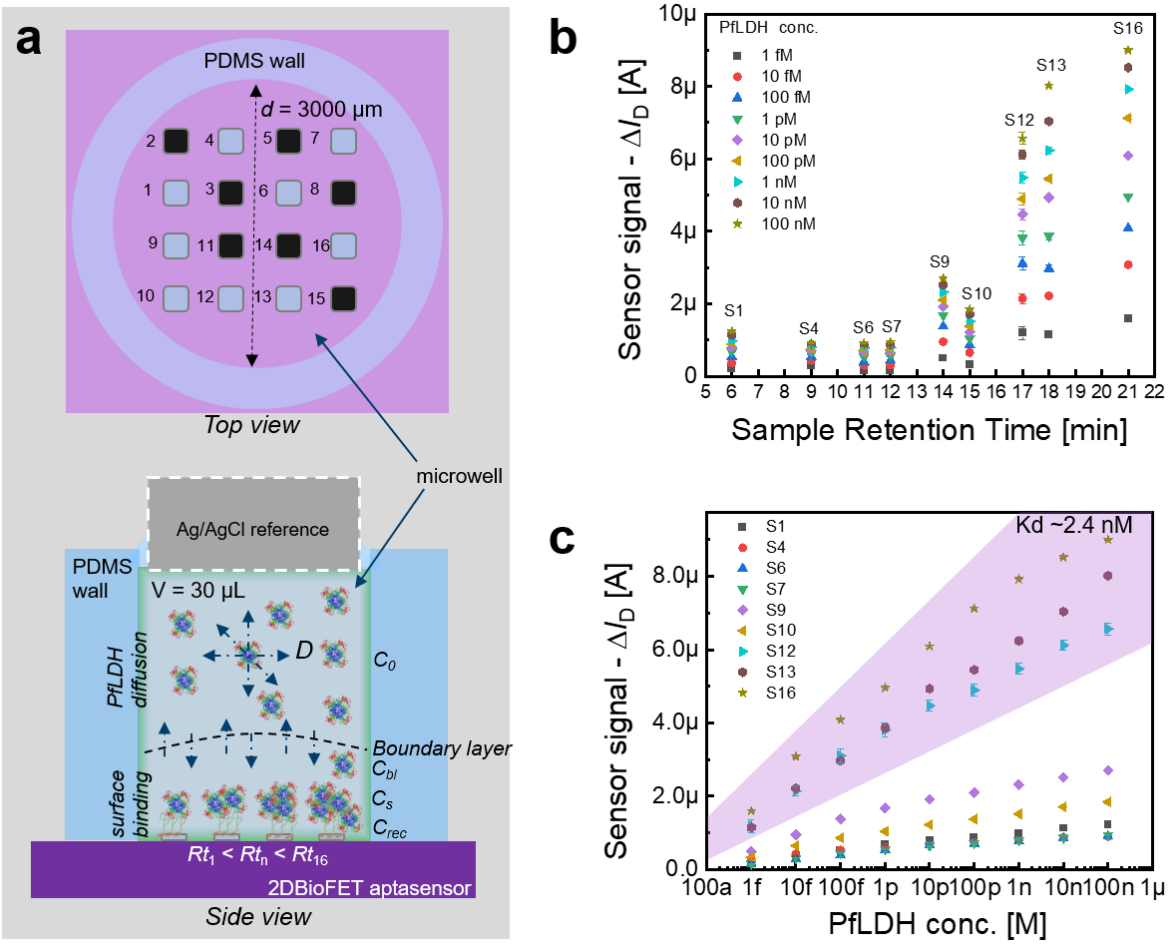

Fig. 3 Sample handling in fluidic microwell and the influence of sample retention time on the bioassay. a Illustrations showing the arrangement of 3 mm diameter PDMS microwells on top of the sensor chip in top-view (above) and side-view (below), which allowed 30 µL sample volumes for analysis and placement of Ag/AgCl reference electrode. The measurements of 2DBioFETs are carried out in a sequence from 1 to 16 to carry out binding analysis. The diffusion-controlled mass transfer process in a fluidic microwell is illustrated in the figure below where the surface density of receptor layer (C_{rec}) and sample retention time (Rt) influence the receptor-analyte interaction. **b** Biosensor signals from 2DBioFETs (S1-S16) for different concentrations of PFLDH in 10 mM PBS at different Rt. Change in the drain-source current output (ΔI_D) at V_D = 100 mV and V_G = -600 mV, with Ag/AgCl as reference, is taken as the biosensor signal of the 2DBioFETs and plotted at the y-axis. The x-axis represents the time duration or Rt for which the given PfLDH concentrations ranging from 1 fM up to 100 nM are maintained in the fluidic microwell. **c** Dose-response curves for different 2DBioFETs with varying Rt are shown in the graph. Binding constants of about 2.4 nM were measured for the 2DBioFETs where PfLDH sample retention times were above 15 min (colored background).

All experiments were repeated with three different chips and nine different 2DBioFETs from each chip (n = 27). C_0: concentration of protein outside the boundary layer; C_{bl}: concentration in boundary layer; C_s: concentration of bound protein to aptamers.

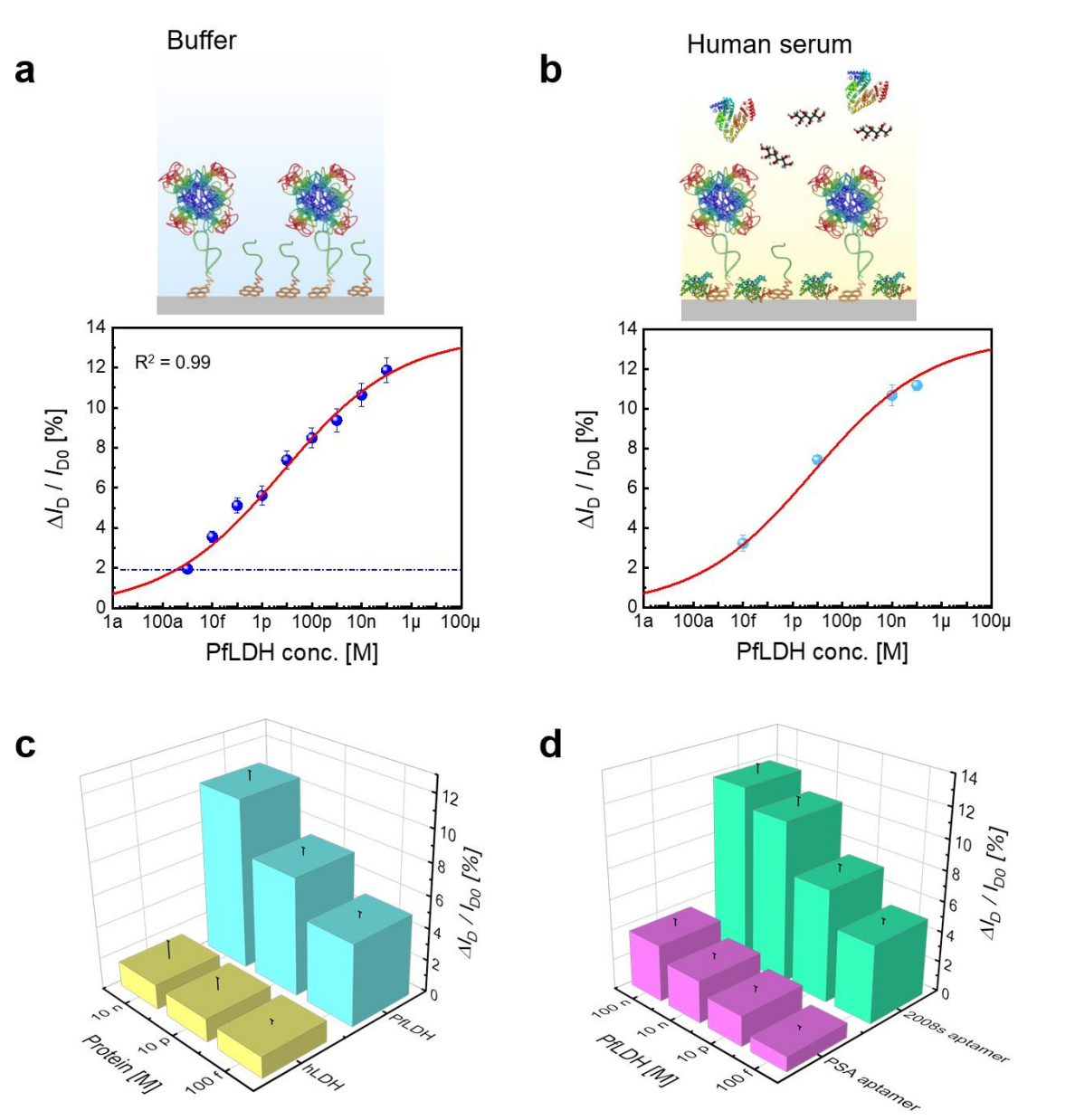

Fig. 4 2DBioFET aptasensor performance and selectivity. a Calibration of the dose-response obtained as the relative percentage of the change in the drain current ($\Delta I_D/I_{D0}$). The red line represents the fit to the Langmuir-Freundlich adsorption isotherm. **b** The plot shows the results of PfLDH detection in human serum by 2DBioFET aptasensor using the standard addition method, which perfectly fits the Langmuir-Freundlich adsorption isotherm curve of the calibration performed in PBS buffer. This 2DBioFET aptasensor contains a BSA blocking step, unlike the PBS buffer condition. **c** Selective PfLDH detection, by 2008s aptamer, proved versus its analogous protein human LDH at three different concentrations for both proteins (100 fM, 10 pM, and 10 nM). **d** The experiment showed the higher specific signal for PfLDH detection by 2008s aptamer when compared with a control aptamer sequence, which was specific for prostate-specific antigens. All experiments were repeated with three different chips and nine different 2DBioF